Initial Developments toward an Active Noise Control System for Small Unmanned Aerial Systems

Noah H. Schiller[a)]
Nikolas S. Zawodny[b)]
NASA Langley Research Center
Hampton, VA 23681, USA

ABSTRACT

Small unmanned aerial systems have the potential to expand commercial markets from package delivery to infrastructure inspection. Many missions, however, require the vehicles to operate in close proximity to people, where community noise concerns could ultimately limit vehicle acceptability. Therefore, noise control technologies may be needed to achieve an acceptable noise signature and enable widespread use of these vehicles. The purpose of this paper is to assess the feasibility of using loudspeakers attached to the vehicle to actively reduce noise. More specifically, this initial study explores the possibility of using a single loudspeaker to reduce the noise from an isolated rotor. Tests performed in an anechoic chamber with a 7.6 cm diameter speaker and 23.9 cm diameter rotor are used to demonstrate the potential benefits and limitations of the concept. Results confirm that active noise control can work in this application with measured tonal reductions of over 30 dB in specific directions. However, since the radiation characteristics of the speaker are different than the rotor, amplification is observed in other directions. This technology has the potential to create a "cone of silence", which could be steered during flight operations to minimize the impact on noise sensitive areas.

1 INTRODUCTION

Small unmanned aerial systems (UAS) are being developed for commercial markets ranging from package delivery to infrastructure inspection. Many missions will require the vehicles to operate in close proximity to people where community noise concerns could ultimately limit vehicle acceptability. Therefore, noise control technologies may be needed to reduce noise exposure and enable widespread use of these vehicles. The purpose of this study is to assess the feasibility of using a loudspeaker attached to the vehicle to actively reduce far-field noise.

Previous studies have focused on characterizing the noise generated by small UAS. Component and subsystem tests have been performed in the laboratory,[1,2] full vehicle tests have been conducted in anechoic chambers,[3,4] and more recently vehicle tests have been performed in

[a)] email: noah.h.schiller@nasa.gov
[b)] email: nikolas.s.zawodny@nasa.gov

an acoustically treated wind tunnel.[5] Field tests have also been performed using several different vehicle configurations.[6,7] Aside from high-frequency tones attributed to the electric motors, most noise from small UAS is due to the rotors.[1,6] Rotor noise can broadly be divided into two categories: rotational noise, and broadband noise.[8] Rotational noise is caused by the thrust (and torque) produced by the rotor, referred to as loading noise, and by the displacement of air as the blades rotate, which is called thickness noise. Loading noise can be steady, relative to an observer on the rotating blade, or unsteady due to a nonzero inflow angle for example. Rotational noise is tonal with well-defined peaks in the measured sound pressure level spectra at the blade passage frequency (BPF) and its harmonics. While the tonal amplitude is typically highest at the BPF, the higher harmonic levels can be significant particularly if there are obstructions in the flow field[2]. Broadband noise, on the other hand, is more random in nature and can be caused, for example, by turbulent flow over the blades. This can be important on small UAS because of the low rotor tip speed. In general, however, the rotor tones still dominate at low frequencies. Therefore, the goal of this study is to assess the feasibility of using active noise control to actively reduce low-frequency tonal noise generated by a small UAS rotor.

Active noise control systems use sensors, typically microphones, along with one or more actuators, often loudspeakers, to measure and attenuate sound. For relatively simple systems that use a single microphone, like the one considered in this study, the response measured by the microphone is referred to as the error signal, since the control objective is to drive the error (i.e., microphone response) to zero. There are different types of control systems that can broadly be divided into either feedback or feedforward architectures. The selection often depends on whether or not an acceptable reference signal is available. To be useful, a reference signal needs to be coherent with the error signal. In other words, there must be some level of linear dependence between the two signals. Typically, feedforward control is used if an acceptable reference is available, while feedback control is used if no reference signal is available. Since the noise generated by many types of small UAS is dominated by rotor tones, as previously discussed, a tachometer (or similar sensor) can be used to provide an acceptable reference signal. Therefore, this study is restricted to feedforward control.

Several research groups have shown that feedforward control systems implemented with loudspeakers can be used to actively reduce the noise generated by rotating fans. One of the first demonstrations was performed by Quinlan,[9] who used a speaker to actively reduce the noise generated by a small axial flow fan with an inlet obstruction. In the test, the reference signal was provided by an infrared tachometer and the error signal was provided by a microphone in the near-field of the fan. Radiated sound power, estimated by measuring pressure on a hemisphere surrounding the setup, was reduced by 12 dB and 7 dB at the blade passage frequency and the second harmonic, respectively. Researchers at Brigham Young University have performed similar tests using multiple speakers in a baffle surrounding a small cooling fan. They also used microphones in the near field of the fan to attenuate far-field noise at harmonics of the blade passage frequency.[10,11] Similar experiments have also been performed by researchers at the University of Sherbrooke using a single unbaffled loudspeaker to attenuate noise from a larger, partially obstructed engine cooling fan.[12,13] Once again, global reductions were achieved at the blade passage frequency. In all cases, local flow obstructions near the fan inlet were used to generate time-invariant flow distortion, resulting in a noise source dominated by unsteady loading noise. This is important to note because researchers have shown that at low frequencies, specifically at low order harmonics of the blade passage frequency, unsteady loading noise radiates similarly to an acoustic dipole.[12] Therefore, a single speaker can be used to match the source characteristics of the fan and achieve global reductions via source coupling.[14]

The purpose of this study is to assess the feasibility of using a single speaker to actively reduce low-frequency tonal noise generated by small UAS. In some cases the sound field may be dominated by unsteady loading noise,[2] but in other cases steady loading and thickness noise may dominate. Therefore, the test setup used in this study consists of a single rotor with no significant flow obstructions. The noise should therefore have significant contributions from steady loading and thickness noise. The paper begins with background information on active noise control, before discussing specific design considerations. A qualitative system model is then discussed, which is subsequently used to help interpret the test results. The experimental setup is described, followed by the results. Finally, some concluding remarks and suggestions for future work are provided.

2 CONTROL DESIGN

The design of an active noise control (ANC) system is application specific. Design variables include the type and placement of control actuators, error sensors, and reference sensors, as well as the selection of the control algorithm and the hardware implementation. To assess system feasibility, it is useful to start with the parameter that has the largest impact on system performance, which is often the control actuators.[15]

The selection and placement of the actuator can be one of the most important decisions impacting the eventual performance of the ANC system. Before selecting the actuator, it is first useful to consider the characteristics of the primary noise source, the rotor in this case. Both the source strength and radiation characteristics (including the directivity and phase response) of the rotor are important. The amplitude and directivity are commonly presented (see Zawodny et al.[1] for example), however, the phase characteristics are discussed less frequently. For steady thickness and loading noise, it is important to note that the sound field rotates in the azimuthal direction.[16,17] In other words, two points equidistant from the rotor hub can have an arbitrary phase offset based on their azimuthal location. Ultimately the amplitude, directivity, and rotating nature of the sound field all have important implications on control performance. Ideally the control actuator would be matched (i.e., collocated with the same radiation characteristics) with the primary source. In that case, it would be possible to simultaneously reduce noise in all directions. If the control actuator is not collocated with the primary source, but is within one-half the acoustic wavelength, then it may still be possible to get global reductions. This is sometimes called source coupling, and is described in the seminal work by Nelson et al.[14] Previous active noise control experiments with axial flow fans achieved global control due to source coupling.

The purpose of this study is to bound the performance that can be achieved using a single loudspeaker. While it may be possible to approximately match the amplitude and directivity, it will not be possible to generate a rotating sound field using a single loudspeaker. Therefore, global control via source coupling is unlikely. Other actuator design parameters are also important, including size, weight, placement, control authority, and frequency response. However, since the goal of this study is simply to establish bounds on the performance of the control system, an oversized speaker was selected for the test.

In addition to the actuator, control systems also typically require error sensors to measure the response of interest. For this study, a single far-field microphone is used as the error signal. While more practical virtual sensing strategies could be used in the future, a far-field microphone is sufficient to establish performance bounds for the system. In addition to the error sensor, a suitable reference sensor is also necessary for feedforward control. In many cases, the signal from a tachometer is correlated with the tonal noise produced by a rotating noise source, and the signal is generally unaffected by the control inputs. Several types of tachometers could be used on a small UAS including brushless RPM sensors, Hall effect sensors, rotary encoders, or optical

tachometers. For this test, a laser tachometer was used to generate a periodic reference signal synchronized with the rotation rate of the rotor.

A standard feedforward controller is used for the assessment. The physical elements of the feedforward control system depicted in Fig. 1 have already been discussed. The reference signal from the tachometer is filtered by the controller. Specifically, current and past samples of the reference signal are multiplied by a vector of filter coefficients to generate the speaker drive signal. The drive signal is filtered by the plant dynamics, which includes both the speaker dynamics and acoustic propagation effects, before it reaches the error microphone. The error microphone measures both the pressure fluctuations generated by the rotor and the loudspeaker. In this test, the standard filtered-reference least mean square (LMS) algorithm was used to update the filter coefficients based on filtered versions of the reference and the error signals to minimize noise at the error microphone. It is useful to note that this type of feedforward system can track changes in motor speed, as captured by the reference signal. This is useful for small UAS applications where differential RPM control is used to fly the vehicle.

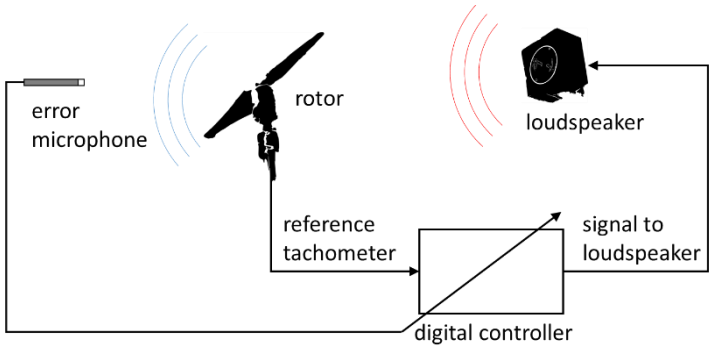

Fig. 1: Feedfoward control system.

3 SIMPLIFIED SYSTEM MODEL

While accurate source models are available for predicting sound radiation from rotating blades, simpler models can often be used for control design. The performance of an active noise control system is often evaluated by looking at the difference between the response (e.g., sound pressure level) with and without control. Therefore, it is not always necessary to predict the absolute level, as long as the relevant source characteristics are captured. Specifically, the model needs to approximate both the directivity and phase characteristics of the sources (rotor and speaker).

The system model used in this study is a three-dimensional acoustic finite element model. The model consists of a hemisphere along with a loudspeaker, approximated by a monopole point source, and a two-dimensional rotor disk. The hemisphere extends 1.9 m from the hub of the rotor disk, which is consistent with the separation distance between the microphones and rotor hub in the test. The amplitude and phase of the monopole, representing the speaker, are determined during the simulation using an iterative process that minimizes the total pressure at a desired error microphone location. The rotor is represented as a spatially-varying circular ring source. Specifically, the incident pressure field on the rotor disk is defined as:

$$p_i = Se^{-imB\theta} \tag{1}$$

where S is a constant source term, m is the harmonic number, B is the blade count, and θ is the azimuthal angle. At the blade passage frequency, the harmonic number is 1, and the azimuthal order, mB, is 2. Similarly, at the second harmonic, the azimuthal order is 4. Equation (1) approximates the noise produced by a rotating disk with a periodic thickness distribution with respect to θ. In other words, it captures the steady thickness noise of a rotor with a high solidity and no axial or edgewise motion. Thickness noise, however, is only one component of the noise produced by a rotating blade, as previously discussed. Steady loading noise is another important component expected during the test. Since sound field plots for thickness and loading noise (as presented by Chapman[17] for instance) have similar phase characteristics, the inclusion of a single, thickness-like source term was deemed sufficient. Once again, the expression given above does not represent a complete source model, but is only intended to capture the relevant complexity of a rotating sound field.

The system response (i.e., acoustic pressure) is found by solving the Helmholtz equation subject to the appropriate boundary conditions.[18] A perfectly matched layer is included around the perimeter of the hemisphere to approximate an anechoic termination. The upper surface of the hemisphere, however, is defined to be acoustically hard to represent a symmetry plane. While the test setup is not perfectly symmetric because the control source is slightly offset from the rotor plane, the offset distance is much less than the acoustic wavelength and was neglected in the simplified model. The acoustic domain was meshed using free tetrahedral quadratic Lagrange elements and the maximum element size was at least eight times smaller than the acoustic wavelength. Near the sources the mesh was much finer, with a maximum element size at least twenty times smaller than the acoustic wavelength. Since the response of an isolated rotor is dominated by tones, the model was solved in the frequency domain at the blade passage frequency (200 Hz) and its harmonics.

4 EXPERIMENTAL SETUP

Tests were performed in the Structural Acoustic Loads and Transmission (SALT) anechoic chamber at the NASA Langley Research Center. The floor, ceiling, and walls of the chamber are covered with approximately 4,850 open-cell polyurethane wedges that are each 0.914 m tall. The wedges reduce acoustic reflections creating a nearly free-field acoustic environment in the chamber down to approximately 100 Hz.[19] The interior dimensions of the chamber are 9.63 m by 7.65 m by 4.57 m tall (measured from wedge tip to wedge tip). A 23.9 cm diameter, 2-bladed rotor driven by a 0.3 kW brushless DC motor was mounted on top of a 3.0 m tall test stand located in the center of the anechoic chamber, as shown in Fig. 2. The rotor is a carbon fiber replica of a DJI 9443 rotor, which is described in more detail in Zawodny et al.[1]

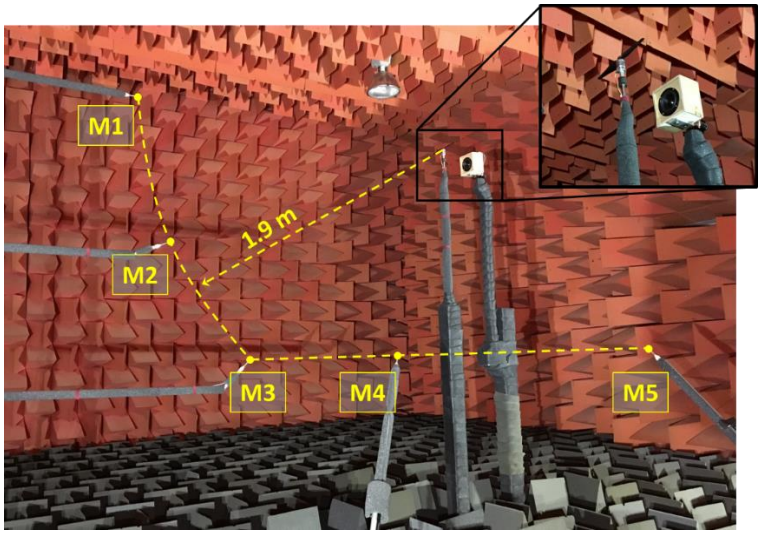

Fig. 2: Test setup in the Structural Acoustic Loads and Transmission anechoic facility at the NASA LaRC.

A 5-element microphone array was used to collect far-field acoustic measurements during the test. Specifically, five 6.35 mm diameter free-field microphones were positioned at a common radial distance, 1.9 m, from the rotor hub. Three elements of the array (labeled M1, M2, and M3) were arranged at a common azimuthal angle, but with different elevation angles of 0°, -22.5°, and -45° relative to the rotor plane. An additional two microphones, labeled M4 and M5, were located at an elevation angle of -45°, but at azimuthal angles of -45° and -90°, relative to M1, M2, and M3. The microphone array is pictured in Fig. 2.

The feedforward control system was implemented on control prototyping hardware with a sample rate of 5 kHz. Eighth-order low pass filters with a cutoff frequency of 1.5 kHz were used as antialiasing and reconstruction filters on the inputs and outputs of the system. The control filter was implemented using a 128-tap FIR filter that was adapted in the time domain using the standard filtered-reference LMS algorithm. The number of filter coefficients, however, was not optimized in this study. Note that while the control system is adaptive, only the converged performance is presented in this paper. Typically, the filter converged in a few seconds. The reference signal was provided by a laser tachometer pointed at the outer casing of the brushless DC electric motor, which spins around the windings. A small piece of reflective tape was placed on the motor housing so the tachometer provided one pulse per revolution of the electric motor. A 7.6 cm diameter speaker installed in a 12.7 cm by 12.7 cm by 8.9 cm deep enclosure was placed on a separate test stand near the rotor. The center of the speaker diaphragm was 19 cm to the right of the rotor hub (away from microphone M1) and 8 cm below the rotor plane. The error signal was obtained from a single far-field microphone. Specifically, microphone M1 was used to provide the error signal in one set of tests and microphone M3 was used in another set of tests.

Before the test, the transfer function from the speaker to the error microphone was identified by playing bandlimited noise from 50-1000 Hz through the speaker, while measuring the microphone response. The input-output relationship representing the plant dynamics was modeled with a 1024-tap FIR filter using a standard Wiener filtering approach.[20]

During the test, the rotational speed of the rotor was set digitally using a USB servo controller connected to the electronic speed controller driving the electric motor. The motor was operated at 6000 revolutions per minute (RPM) during all tests, which corresponds to a blade passage frequency (BPF) of 200 Hz. The tests were performed in a closed anechoic chamber. Therefore, inflow variations caused by flow recirculation within the chamber introduced additional unsteady

loading noise resulting in temporal modulation and increased harmonic content. Atmospheric turbulence would likely generate a similar effect during flight. So, instead of limiting the run time to avoid this effect, the rotor was allowed to operate for at least 30 seconds before any data was collected. This was done in an attempt to reach a quasisteady condition where the inlet turbulence could be approximated as a stationary random process. Data was then acquired at a sample rate of 20 kHz for a duration of 10 seconds with the control system off. Finally, the control system was turned on, given a few seconds to converge, and an additional 10 seconds of data was collected.

5 RESULTS

The results are divided into two subsections. The characteristics of the measured sound field are discussed first, followed by predictions and measurements of the control performance. Two sets of control results are presented with either M1 or M5 as the error microphone.

5.1 Sound Field Characteristics

The sound pressure level spectra for M1, M3, and M5 are shown in Fig. 3(a). These microphones are located at the corners of the array and generally bound the measured response. The spectra are dominated by tones, particularly at the BPF (i.e., 200 Hz) and at higher harmonics (i.e., 400 Hz, 600 Hz, 800 Hz, etc.) of that frequency. A lower amplitude tone is present at the shaft rotation rate, 100 Hz, which is indicative of blade imbalance. Odd multiples of the shaft rotation rate are also present, but are typically lower amplitude than the BPF related tones. The spectra has more harmonic content than previously published results acquired on an isolated rotor.[1] The difference is attributed to the addition of the test stand and speaker, which introduce azimuthal variation in the flow field. The blade passage frequency is, however, still dominant.

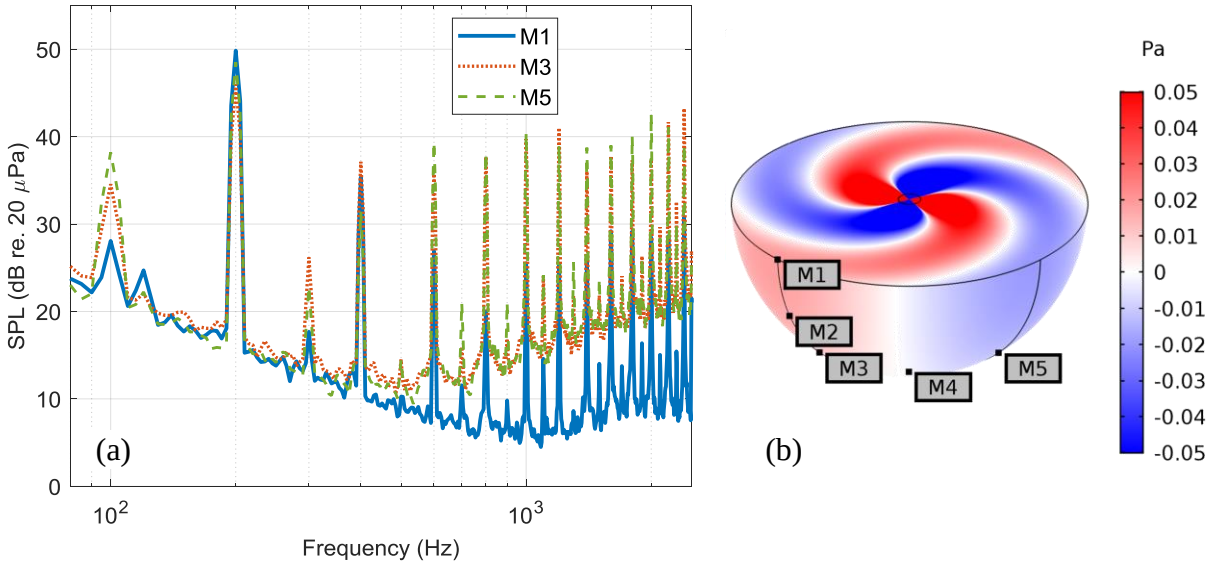

Fig. 3: (a) Sound pressure level spectra measured at microphones M1, M2, and M3, and (b) predicted pressure field at the blade passage frequency.

The sound pressure level plots provide important information about the frequency content, amplitude, and directivity of the rotor, but provide no information regarding phase. Since the phase of the pressure field is important to the overall performance of the control system, it needs to be

considered as well. Predictions are helpful to understand the expected phase characteristics of the sound field and interpret the phase measurements. For example, Fig. 3b) shows the predicted pressure field radiating from a spinning disk. The image shows the characteristic swirling pattern generated by a spinning source rotating in the counter clockwise direction (from above) along with the location of each microphone. It is clear that the phase will vary in a spinning sound field, particularly at microphones M3, M4, and M5.

Comparisons of the measured and predicted phase at the five microphone locations are shown in Fig. 4. Both predictions and measurement are included for the lowest three harmonics of the BPF. In all cases the phase is shown relative to the response at M1. At the blade passage frequency, the measured phase is similar to the predictions generated from the sound field shown in Fig. 3b). Specifically, the pressure fluctuations generated by the spinning source disk are measured almost simultaneously by M1-M3, followed by M4, and finally by M5. Furthermore, the phase difference between M1 and M4 is -90° and the difference between M1 and M5 is approximately -180°. The comparison between predictions and measurements is not as good at the second harmonic. The model predicts a phase difference of -180° between M1 and M4, and -360° (wrapped to 0°) between M1 and M5. The measurements, however, show a nearly flat phase response, which is similar to the phase behavior of a stationary monopole centered in the middle of the source disk. Similar differences are observed at the third harmonic. The predictions for M4 and M5 are -270° (wrapped to +90°) and -540° (wrapped to -180°), respectively. The measured phase behavior is again similar to a stationary monopole, but now the apparent source location is below the rotor disk. To summarize, the simple numerical model appears to capture the relevant phase characteristics at the BPF, but does not capture the phase behavior at higher harmonics. Furthermore, the measured phase behavior of the higher harmonics is not indicative of a spinning sound field, but instead the rotor appears to radiate more like a stationary monopole. It is possible that the azimuthal variation in the flow field (introduced by the speaker and support stand) results in significant unsteady loading noise at the higher harmonics. Unsteady loading noise does not radiate in the same way as steady thickness and loading noise, but instead appears to radiate more like a monopole. The radiation response of the control speaker is considered next.

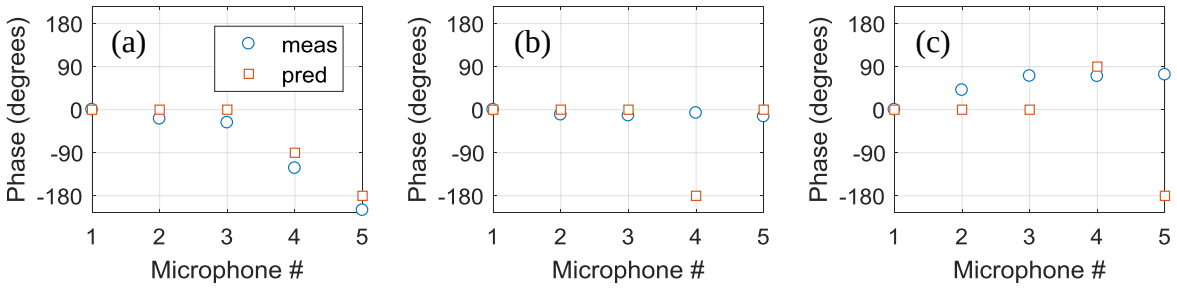

Fig. 4: Phase of the sound field generated by the rotor at: (a) the BPF, (b) 2x the BPF, and (c) 3x the BPF. Measurements are shown with blue circles and predictions are shown with red squares. Phase is relative to microphone #1.

The predicted phase response of the speaker, modeled as a monopole placed at the appropriate location relative to the rotor hub, is shown in Fig. 5. At the BPF, the phase response is relatively flat. At the higher harmonics, the acoustic wavelength is shorter and the phase difference between the microphones is more obvious. The phase accumulation is due to the fact that the microphones are not equidistant from the monopole since the source is offset from the rotor hub. By comparing Fig. 4(a) and Fig. 5(a), it is clear that the phase behavior of the rotor and speaker are different at the BPF. This mismatch in the phase behavior imposes a fundamental limit on the performance of

the active noise control system. Attenuation in one direction will always result in amplification in other directions. The same is not true, however, at the higher harmonics. For example, at the third harmonic, the phase characteristics of the speaker are similar to the measured phase characteristics of the rotor. Therefore, the response could theoretically be reduced simultaneously at all microphone locations (if the amplitude and directivity also match at this frequency).

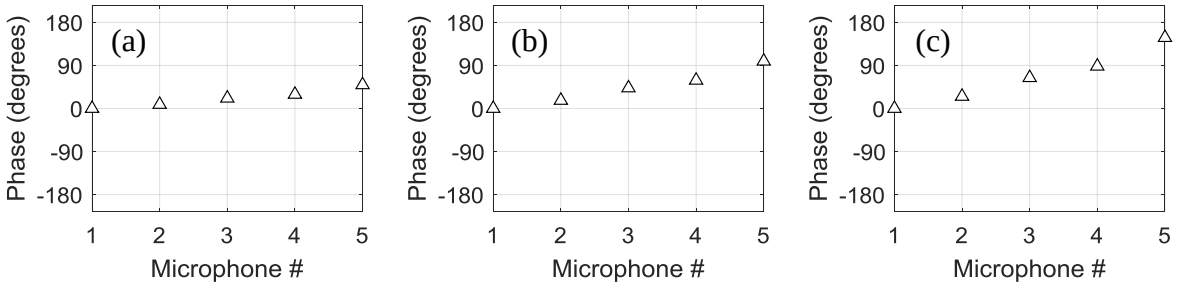

Fig. 5: Theoretical phase response for an offset monopole at: (a) the BPF, (b) 2x the BPF, and (c) 3x the BPF. Phase is relative to microphone #1.

5.2 Control Performance

Results are included for two different control cases. In one case, M1 is used as the error microphone, and in the second case, M5 is used as the error microphone. Predictions for both cases are shown in Fig. 6. Specifically, the change in sound pressure level due to the active noise control system is shown on a hemisphere below the rotor disk. The rotor is indicated by the small circle on the top surface of the hemisphere and the speaker is indicated by the small green dot near the rotor disk. The five microphone locations are also labeled. Since the model does not capture the measured phase behavior at the higher harmonics, predictions are only provided at the BPF. Microphone M1 was used as the error microphone in Fig. 6(a), while M5 was used as the error microphone in Fig. 6(b). The predictions show that attenuation is achieved near the error microphone in exchange for amplification in other regions. This is a direct result of the phase mismatch between the speaker and rotor, as previously discussed.

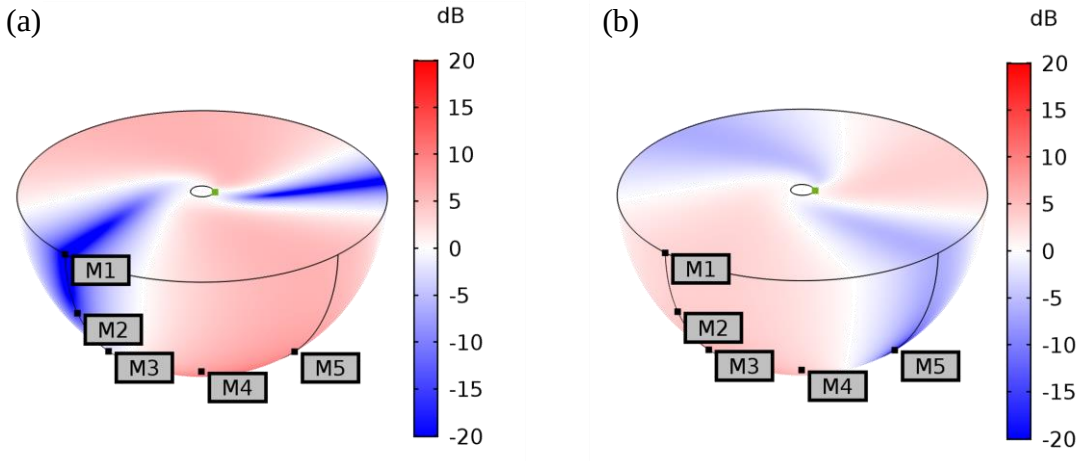

Fig. 6: Predicted change in the SPL at the BPF with an active noise control system using an error microphone at (a) M1 or (b) M5.

Measured results are presented next. Before implementing a feedforward control system, the coherence between the reference and error signals can be used to establish bounds on the expected performance. In this case, the coherence exceeded 0.9 at the first three harmonics of the BPF, which implies that more than 10 dB of attenuation is possible using feedforward control. Therefore, the real-time control system was implemented and tested. Control performance was initially evaluated using M1 as the error sensor. The measured sound pressure level spectra for this case are shown for M1, M3, and M5 in Fig. 7. At the BPF (i.e., 200 Hz), a significant reduction was achieved at M1 in exchange for amplification at M3 and M5. This finding is consistent with the predictions shown in Fig. 6(a). The spatial extent of the quiet zone is larger at the higher harmonics. For example, attenuation at the second harmonic (i.e., 400 Hz) is achieved at both M1 and M3 with minimal amplification at M5. At the third harmonic (i.e., 600 Hz), attenuation is achieved at all microphones in the array, not just the three shown in Fig. 7. The large spatial extent of the quiet zone observed at this frequency is attributed to the favorable phase match between the speaker and rotor. It is useful to note that since the sound field is tonally dominated, the overall sound pressure level integrated from 80 Hz through 5000 Hz was reduced by 8 dB at M1 and 2 dB at M2. However, the overall sound pressure level was unchanged at M3 and increased by 3 dB and 2 dB at M4 and M5, respectively. It may also be useful to note that during operation the electrical power required to operate the loudspeaker was approximately 10 mW, which was more than two orders of magnitude less than the power draw of the electric motor.

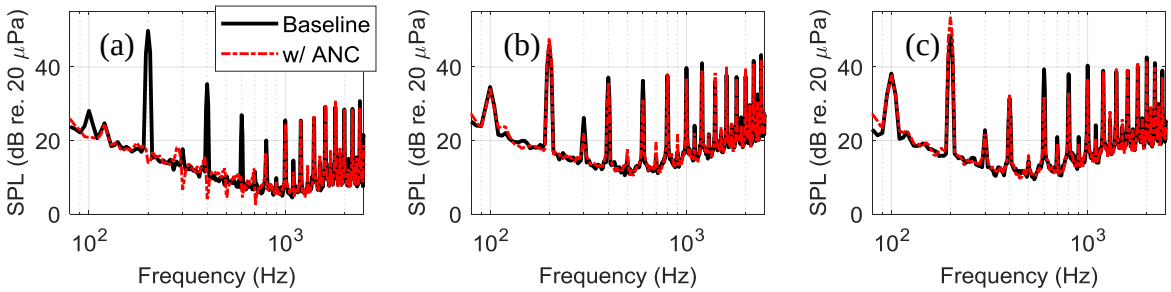

Fig. 7: Measured sound pressure level without control (shown by the solid black curves) at (a) M1, (b) M3, and (c) M5 along with measured results with the active noise control system (shown by the dashed red curves). The error microphone was positioned at M1.

Next, the control results are presented using M5 as the error sensor. The corresponding sound pressure level spectra are shown for M1, M3, and M5 in Fig. 8. Significant attenuation was achieved at M5 in exchange for amplification at the other microphone locations. The predictions, shown in Fig. 6(b), capture the trends observed in the measurements at the BPF. Once again, the tonal attenuation at the BPF appears to be limited due to the mismatch between the phase characteristics of the speaker and rotor. In contrast, attenuation at the second harmonic is achieved with minimal amplification at other microphone locations. Attenuation at the third harmonic is not achieved at all microphone locations, in contrast to previous results with M1 as the error sensor. While the speaker and rotor have similar phase characteristics, directivity differences degraded the control performance in this case. To get significant attenuation, the speaker needs to generate pressure fluctuations that are comparable in amplitude and out-of-phase with the rotor. Since the amplitude of the rotor response at the error microphone, M5, is larger than the response at M1 and M3, yet the speaker has a nearly constant amplitude response, amplification was observed despite the favorable phase relationship.

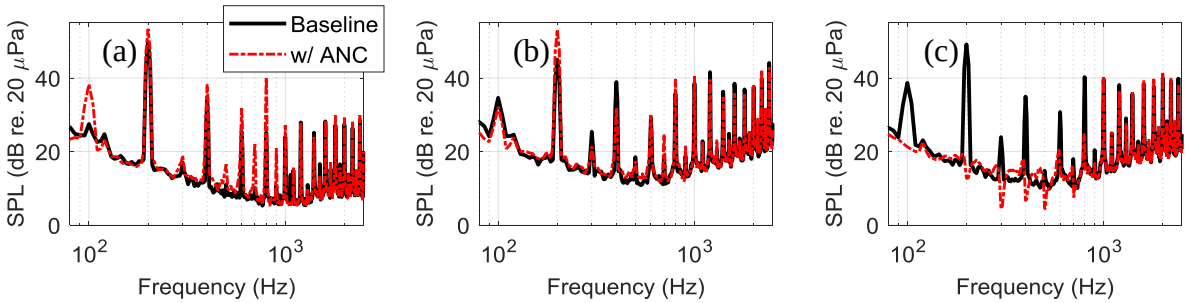

Fig. 8: Measured sound pressure level without control (shown by the solid black curves) at (a) M1, (b) M3, and (c) M5 along with measured results with the active noise control system (shown by the dashed red curves). The error microphone was positioned at M5.

The results are distilled further in Table 1, which compares the change in the tonal sound pressure level with and without the active noise control system. The numbers in red highlight the frequencies and microphones where attenuation was achieved, while the numbers in black correspond to amplification. As previously discussed, the spatial extent of the quiet zones was often larger at the higher harmonics because the source matching between the rotor and speaker improved.

Table 1 - Change in measured tonal sound pressure level using the ANC system with the error microphone at (a) M1 or (b) M5.

(a) Delta SPL (dB) using error signal from M1

	BPF (200 Hz)	2x BPF (400 Hz)	3x BPF (600 Hz)
M1	-36	-31	-20
M2	-7	-8	-5
M3	+2	-2	-5
M4	+6	+1	-7
M5	+5	+1	-8

(b) Delta SPL (dB) using error signal from M5

	BPF (200 Hz)	2x BPF (400 Hz)	3x BPF (600 Hz)
M1	+4	+4	+6
M2	+5	-1	+6
M3	+8	-7	+1
M4	+4	-3	-1
M5	-37	-28	-16

6 CONCLUDING REMARKS

Results confirm that active noise control can be used to reduce the noise from small rotors with measured tonal reductions of over 30 dB at specific microphone locations. However, since the radiation characteristics of the speaker are different than the rotor at the blade passage frequency, attenuation is achieved in some directions in exchange for amplification in other directions. Similar trends are captured using a simplified numerical model. At higher harmonics, the measured phase characteristics of the rotor are similar to a stationary point source, and attenuation is achieved over a wider range of directions. The ability to attenuate noise in specific directions could be useful, particularly if the vehicle is able to monitor its surroundings and then steer the "cone of silence" during operation to minimize its impact on noise-sensitive areas. Future active noise control work will target higher harmonics of the BPF, which are anticipated to be more pronounced when flow obstructions are present in the inflow or exhaust. This will relax the speaker size requirements and potentially enable the use of speakers embedded in the vehicle body. The focus on high frequency tones may also have a larger impact on community acceptance. On-vehicle error sensors are also being considered for this application.

8 REFERENCES

1. N. S. Zawodny, D. D. Boyd Jr., C. L. Burley, "Acoustic characterization and prediction of representative, small-scale rotary-wing unmanned aircraft system components," in *Proceedings of the AHS 72nd Annual Forum*, (West Palm Beach, FL), May 2016.
2. N. S. Zawodny, D. D. Boyd Jr., "Investigation of rotor-airframe interaction noise associated with small-scale rotary-wing unmanned aircraft systems," in *Proceedings of the AHS 73rd Annual Forum*, (Ft. Worth, TX), May 2017.
3. N. Intaratep, W. N. Alexander, W. J. Devenport, S. M. Grace, A. Dropkin, "Experimental study of quadcopter acoustics and performance at static thrust conditions," in *Proceedings of the 22nd AIAA/CEAS Aeroacoustics Conference*, (Lyon, France), May 2016.
4. K. Herreman, "Proposed measurement method for UAV sound levels," in *Proceedings of NoiseCon 2016*, (Providence, RI), June 2016.
5. N. S. Zawodny, N. A. Pettingill, "Acoustic wind tunnel measurements of a quadcopter in hover and forward flight conditions," in *Proceedings of InterNoise 2018*, (Chicago, IL), Aug. 2018.
6. R. Cabell, R. McSwain, R., F. Grosveld, "Measured noise from small unmanned aerial vehicles," in *Proceedings of Noise-Con 2016*, (Providence, RI), June 2016.
7. A. Christian, R. Cabell, "Initial investigation into the psychoacoustic properties of small unmanned aerial system noise," in *Proceedings of the 23rd AIAA/CEAS Aeroacoustics Conference*, (Denver, CO), June 2017.
8. F. H. Schmitz, "Rotor Noise," Chapter 2 in *Aeroacoustics of Flight Vehicles: Theory and Practice: Volume 1: Noise Sources*, edited by H. H. Hubbard, NASA RP-1258, (1991).
9. D. A. Quinlan, ''Application of active control to axial flow fans,'' *Noise Control Eng. J.*, **39**(3), 95–101, (1992).
10. K. L. Gee, S. D. Sommerfeldt, "Application of theoretical modeling to multichannel active control of cooling fan noise," *J. Acoust. Soc. Am.*, **115**(1), 228-236, (2004)
11. R. L. Rust, S. D. Sommerfeldt, K. L. Gee, J. D. Blotter, "Characterization of microphone placement and noise sensitivity in a global active noise control system for a compact noise source," *Noise Control and Eng. J.*, **61**(3), 280-290, (2013).
12. A. Gerard, A. Berry, P. Masson, "Control of tonal noise from subsonic axial fan. Part 1: Reconstruction of aeroacoustic sources from far-field sound pressure," *J. Sound and Vib.*, **288**, 1049-1075, (2005).
13. A. Gerard, A. Berry, P. Masson, "Control of tonal noise from subsonic axial fan. Part 2: Active control simulations and experiments in free field," *J. Sound and Vib.*, **288**, 1077-1104, (2005).
14. P. A. Nelson, A. R. D. Curtis, S. J. Elliott, A. J. Bullmore, "The minimum power output of free field point sources and the active control of sound," *J. Sound and Vib.*, **116**(3), 397-414, (1987).
15. C. Hansen, S. Snyder, X. Qiu, L. Brooks, D. Moreau, *Active Control of Noise and Vibration, Second Edition*, CRC Press, Boca Raton, FL, (2012).
16. P. R. Prentice, "The acoustic ring source and its application to propeller acoustics," *Proc. R. Soc. Lond. A*, **437**, 629-644, (1992).
17. C. J. Chapman, "The structure of rotating sound fields," *Proc. R. Soc. Lond. A*, **440**, 257-271, (1993).
18. COMSOL Multiphysics Modeling Software, Ver. 5.3, 2017.
19. F. W. Grosveld, "Calibration of the Structural Acoustics Loads and Transmission Facility at NASA Langley Research Center," in *Proceedings of InterNoise 99*, (Ft. Lauderdale, FL), Dec. 1999.
20. S. J. Elliott, *Signal processing for active control*, Academic Press, London, (2001).